EGU2020: Sharing Geoscience Online - EGU2020-6669

Fracture characterisation using frequency-dependent shear-wave splitting analysis of azimuthal anisotropy: application to fluid flow pathways at the Scanner Pockmark area, North Sea

A.H. Robinson[1] (contact: a.h.robinson@soton.ac.uk), G. Bayracki[1,2], C. MacDonald[3], B. Callow[1], G. Provenzano[1], T.A. Minshull[1], M. Chapman[3], T. Henstock[1], J. M. Bull[1]

[1]Ocean and Earth Science, University of Southampton, National Oceanography Centre Southampton, SO14 3ZH, U.K
[2]National Oceanography Centre Southampton, Southampton, SO14 3ZH, U.K.
[3]School of Geosciences, University of Edinburgh, EH9 3JW, U.K.

This project has received funding from the NERC (CHIMNEY, NE/NO16130/1) and the European Union's Horizon 2020 research and innovation programme (STEMM-CCS) under grant agreement No. 654462

Conceptual model of seismic chimney structures

Figure **(right)** shows the proposed geometry for the crack networks associated with chimney structures.

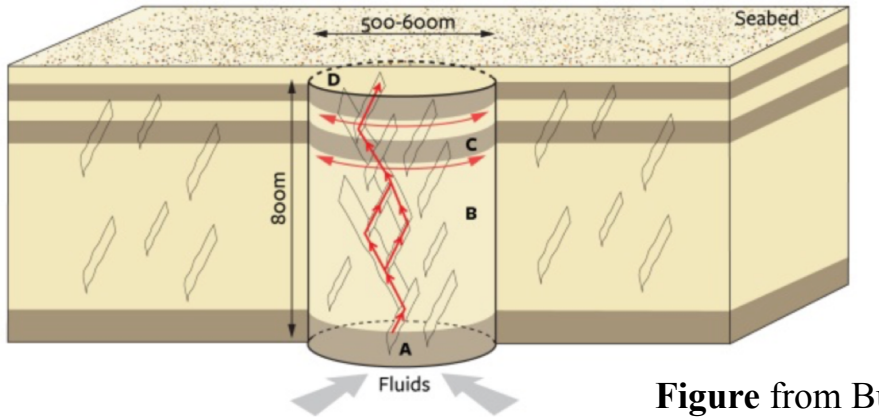

Figure from Bull et al. (2018)

Comprises unconnected vertical fractures outside the chimney, preferentially aligned with the regional stress field, and a more connected, possibly concentric fracture system within the chimney.

If this is the case, we would therefore **expect to observe variations in the anisotropy measured inside and outside of the chimney**.

The CHIMNEY project tests this hypothesis at Scanner pockmark, North Sea, using a broad-frequency-range seismic experiment, to attempt to identity anisotropy using observations of shear wave splitting (SWS).

Seismic chimney at Scanner Pockmark, North Sea

Multichannel seismic reflection profiles collected with GI guns and surface sparker sources (e.g. figure, right)

Used to constrain the subsurface structure beneath and around Scanner pockmark.

Amplitude bright spots (lower panel) and blanking of seismic amplitudes below these (upper panel, within Aberdeen Ground Fm.) indicate presence of gas in the subsurface, both at seabed immediately beneath pockmark, and at top of a vertically oriented seismic chimney in the subsurface.

Active venting of methane from the seabed is ongoing at Scanner pockmark, at a rate of ~150 L/min (Roche & Li, pers. comm.).

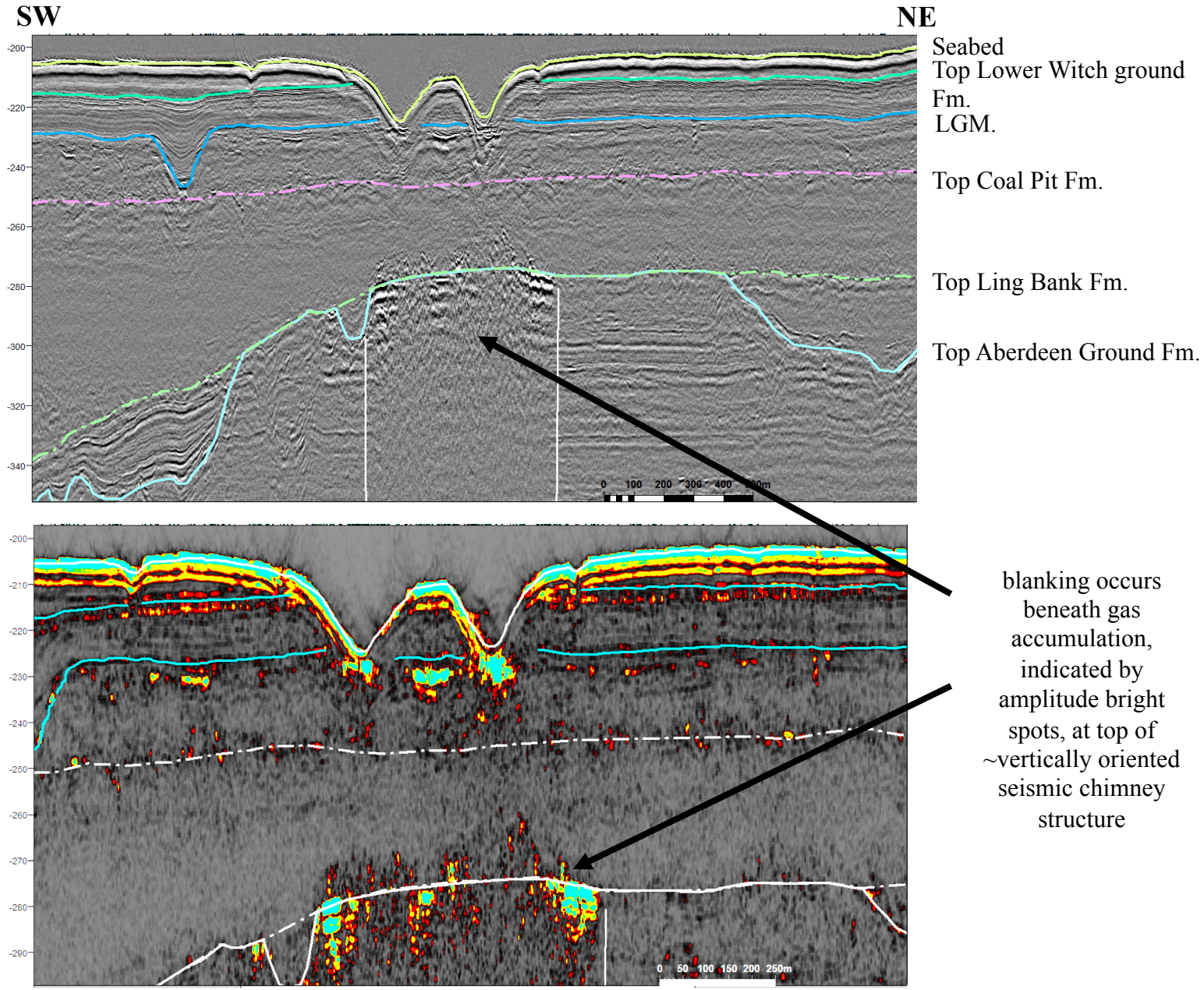

Figure: Sparker seismic reflection section traversing Scanner pockmark (above) and extracted RMS amplitudes (below), vertical exaggeration 10

Principles of shear-wave splitting (SWS) analysis

SWS occurs when a polarized shear-wave enters an anisotropic medium, causing it to split into two shear-waves polarized in the fast (S_1) and slow (S_2) directions (figure, below).

Orientations and properties of the cracks in the medium can be determined by analysis of the directions of the polarizations and time delay between the two phases.

Where SWS occurs, characteristic patterns in signal amplitude and polarity are observed on the radial (direction of shot from receiver and transverse (perpendicular to R) components.

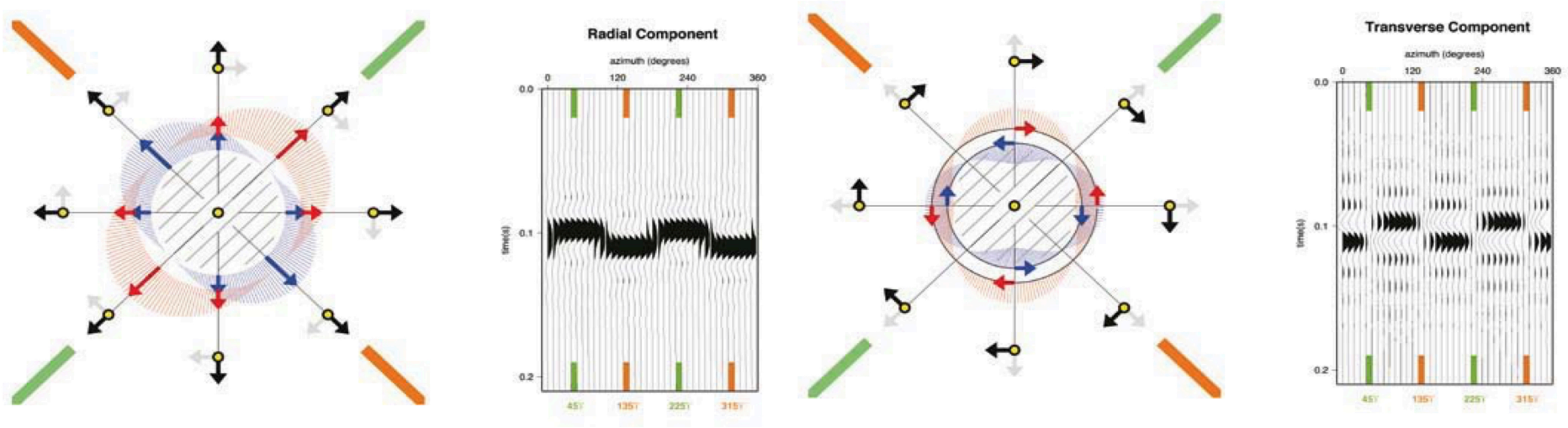

Figure from Bale et al. (2009) showing SWS patterns for an HTI medium (vertically oriented fractures). Orange and green lines represent symmetry planes of SWS. Note the characteristic 90˚/180˚ patterns in the radial and transverse components associated with the symmetry planes.

Frequency Dependent Anisotropy

Frequency dependent approach to studying anisotropy is required due to differing sensitivity of different fracture sizes to signal frequency (Chapman, 2003; **fig. right**).

Also potential ambiguity between medium containing a small number of large fractures versus a larger number of smaller fractures, which will produce similar responses (e.g., Maultzsch et al., 2003) due to similar crack density.

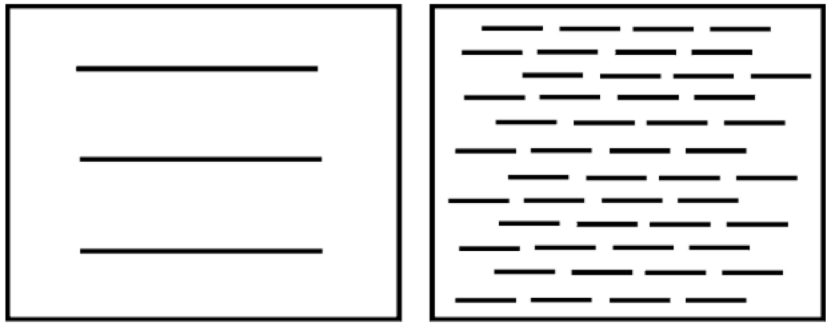

Figure 1 The same crack density can be caused by a few large fractures as shown on the left or many small cracks as shown on the right.

Figure from Maultzsch et al., (2003)

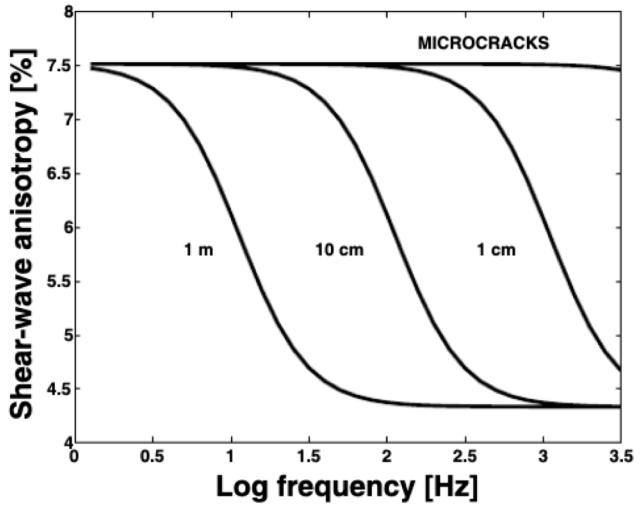

Figure 7 Shear-wave anisotropy as a function of frequency for various fracture sizes, with 10% equant porosity and a crack density of 0.1. Propagation is at 70° to the fracture normal.

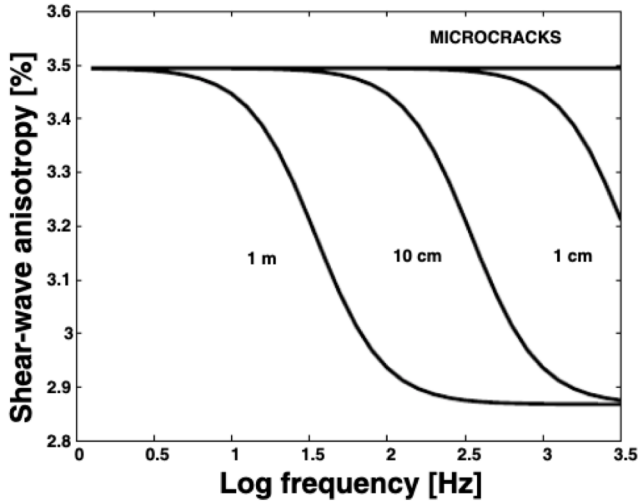

Figure 8 Shear-wave anisotropy as a function of frequency for various fracture sizes, with 0% equant porosity and a crack density of 0.02. Propagation is at 70° to the fracture normal.

Figure from Chapman (2003)

Scanner Pockmark anisotropy experiment, North Sea (Bull, 2017)

This experiment was specifically designed for the study of frequency dependent seismic anisotropy.

- 5 seismic sources used, with broad frequency range of 5-3000 Hz.
- Data recorded on OBSs with hydrophone and three-component geophone. Locations indicated by triangles
  - 18 around pockmark, inc. 2 inside
  - 7 at nearby reference site
- Profiles acquired covering a wide range of azimuths (black sail lines) over the array.

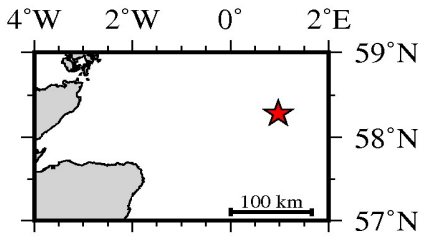

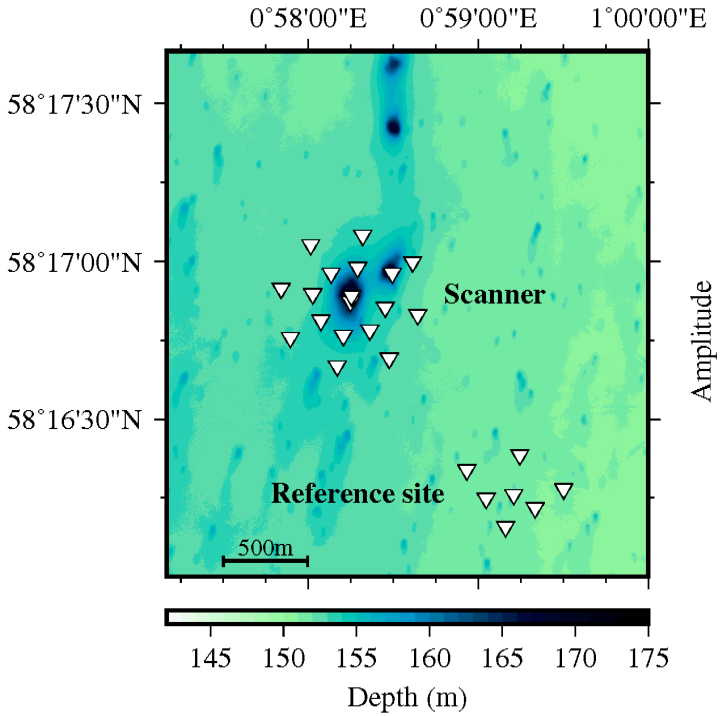

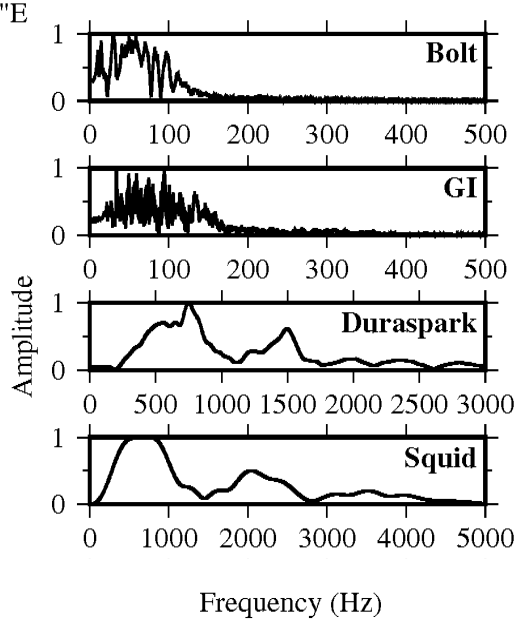

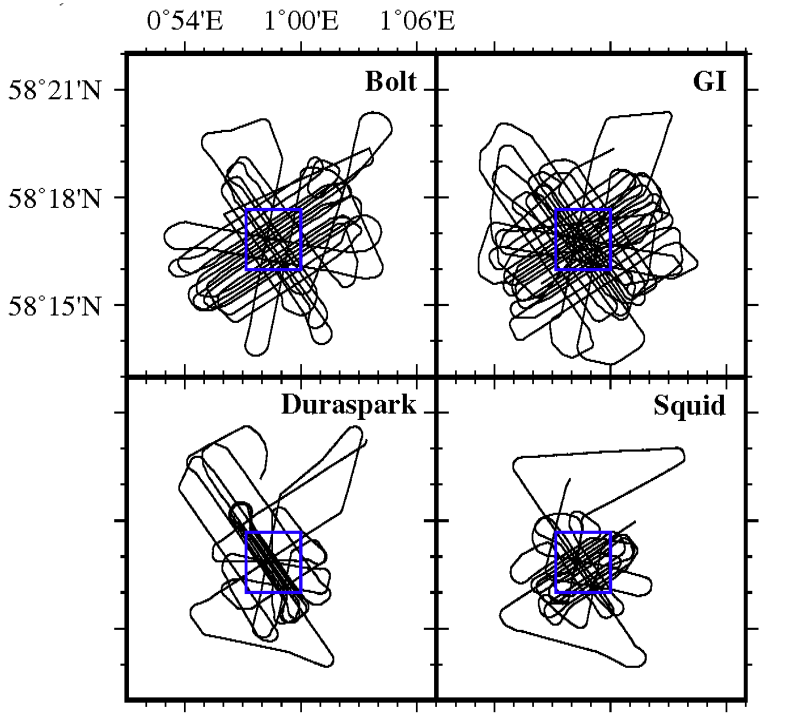

Blue box corresponds to region shown in map to left

Our data processing scheme follows that of Haacke & Westbrook (2006) and Exley et al. (2010).

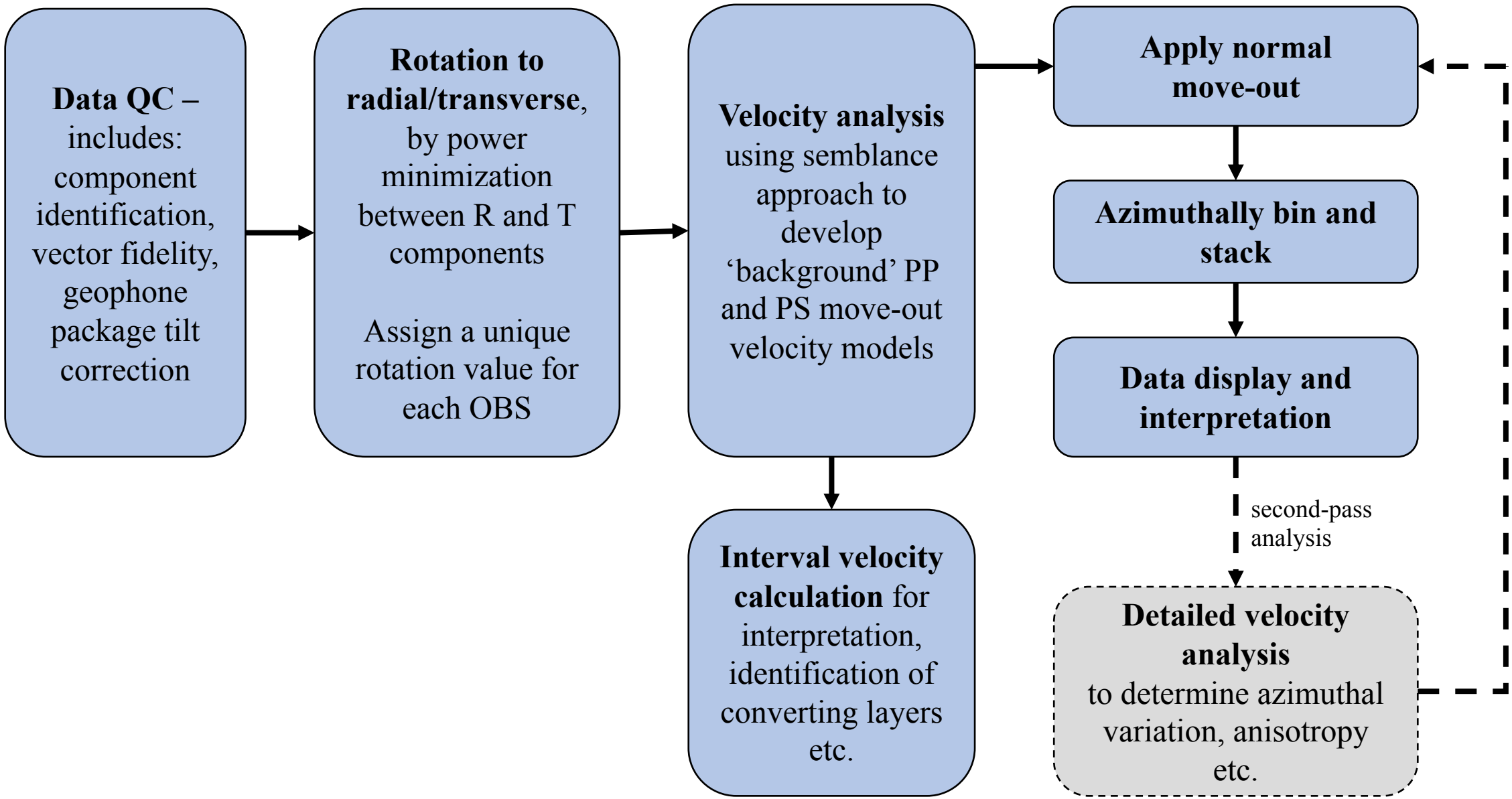

Move-out velocity analysis radial component

Move-out velocity trends for whole dataset picked on:

- PP (black dashed on semblance panels) - *Duraspark H, GI H (back up GI, Z)*
- PS (black solid) - *GI and Bolt R (back up GI and Bolt Z)*

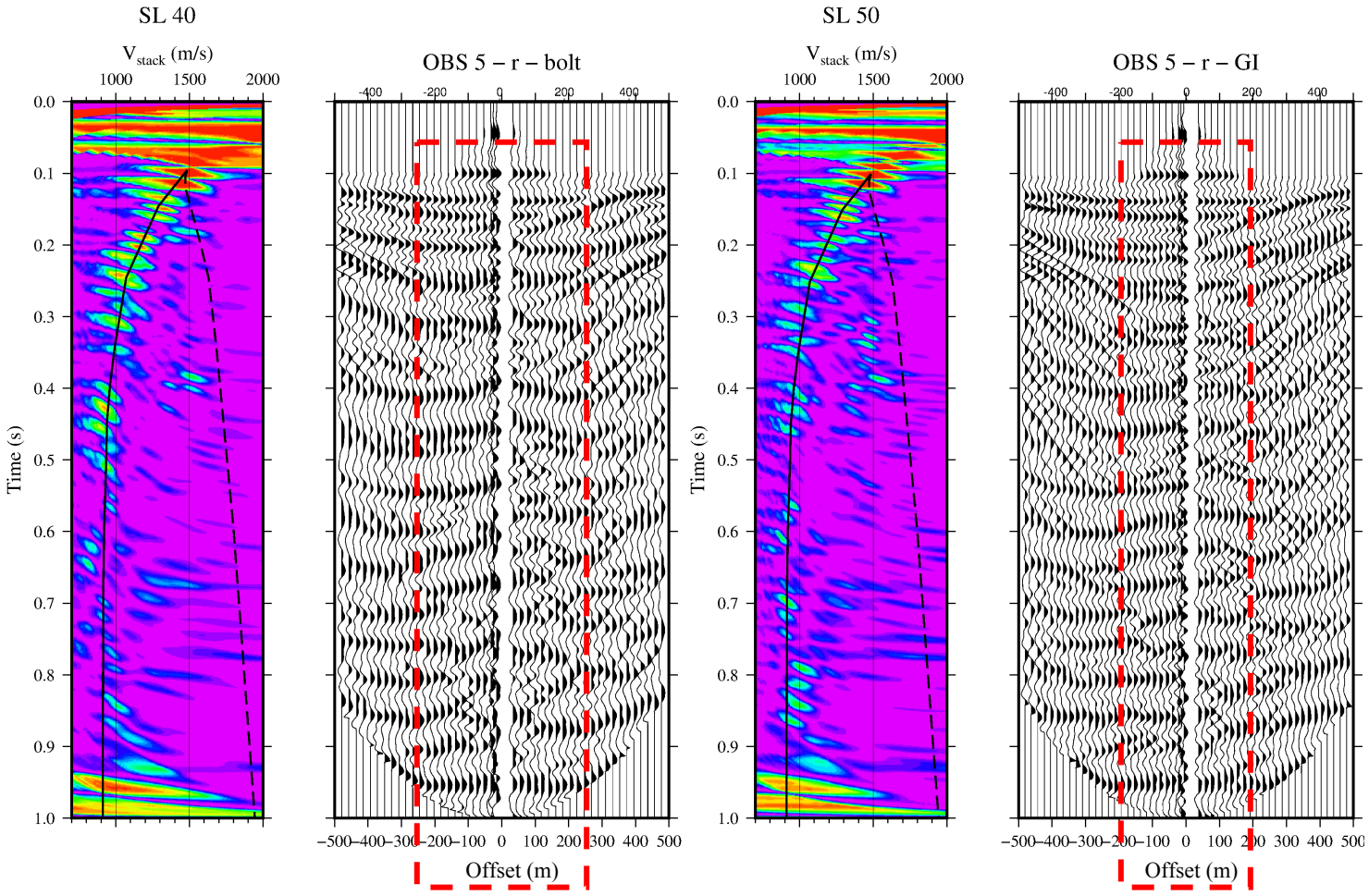

semblance (left) and PS move-out corrected gathers (right) for OBS 5, radial component, Bolt and GI sources

10-20-50-75 Hz bandpass filter and time-amplitude correction applied to data

'Background' trends show good correspondence with semblance peaks, suitable for first-stage move-out application and data inspection.

Note that velocity analysis and move-out as applied here are hyperbolic, while P-S converted arrivals result in non-hyperbolic arrival trends. However, for limited offset ranges, this is a suitable first-pass assumption (Stewart & Ferguson, 1996).

Strong semblance trend in R component, with V_{stack} decreasing from 1485-1490 to ~900 m/s indicates presence of converted P-S arrivals.

Regions highlighted in red display good flattening of arrival events, between ~0.1 s (direct arrival) and ~0.5 s.

These offset ranges also exclude arrivals which show characteristics suggestive of refractive origin.

Move-out velocity analysis
transverse component

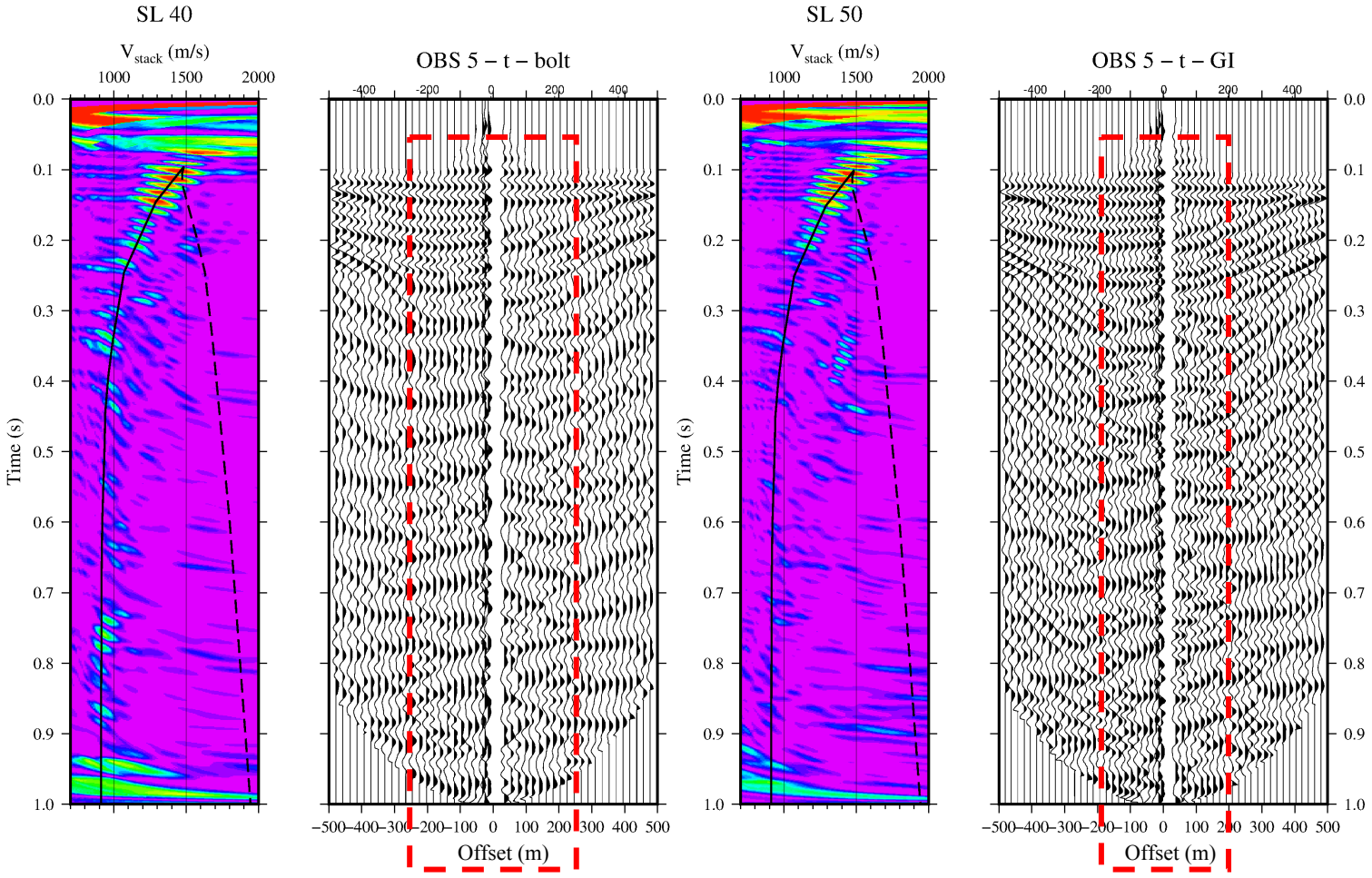

semblance (left) and PS move-out corrected gathers (right) for OBS 5, transverse component, Bolt and GI sources

10-20-50-75 Hz bandpass filter and time-amplitude correction applied to data

Transverse component semblance peaks strongest up to 0.1-0.15 s after direct arrival (at ~0.1 s).

PS move-out corrected gathers show flattening of candidate S-wave arrivals in T component to offsets of ~200-300 m.

Due to the polarity reversal characteristic of SWS observed in T components, coherent stacking of this component is less sensitive to inexact move-out, particularly at lower frequencies.

A background move-out velocity model can be used to identify orientations of symmetry planes and average velocity-depth structure, and can then be refined to improve flattening, particularly of R component (Exley et al., 2010).

Interval velocity

P wave interval velocity (Vp_{int}) is calculated from PP move-out trend using a standard Dix (1955) approach
S wave interval velocity (Vs_{int}) is calculated from PS move-out trend and Vp_{int} using a modified Dix approach by Stewart & Ferguson (1996)

Note: the jagged/irregular nature of Vs_{int} likely results from the sampling regularity of the velocity-time trends used as an input

Black = PS move-out velocity

Solid red = PP move-out velocity
Dashed red = PP interval velocity (Dix converted)

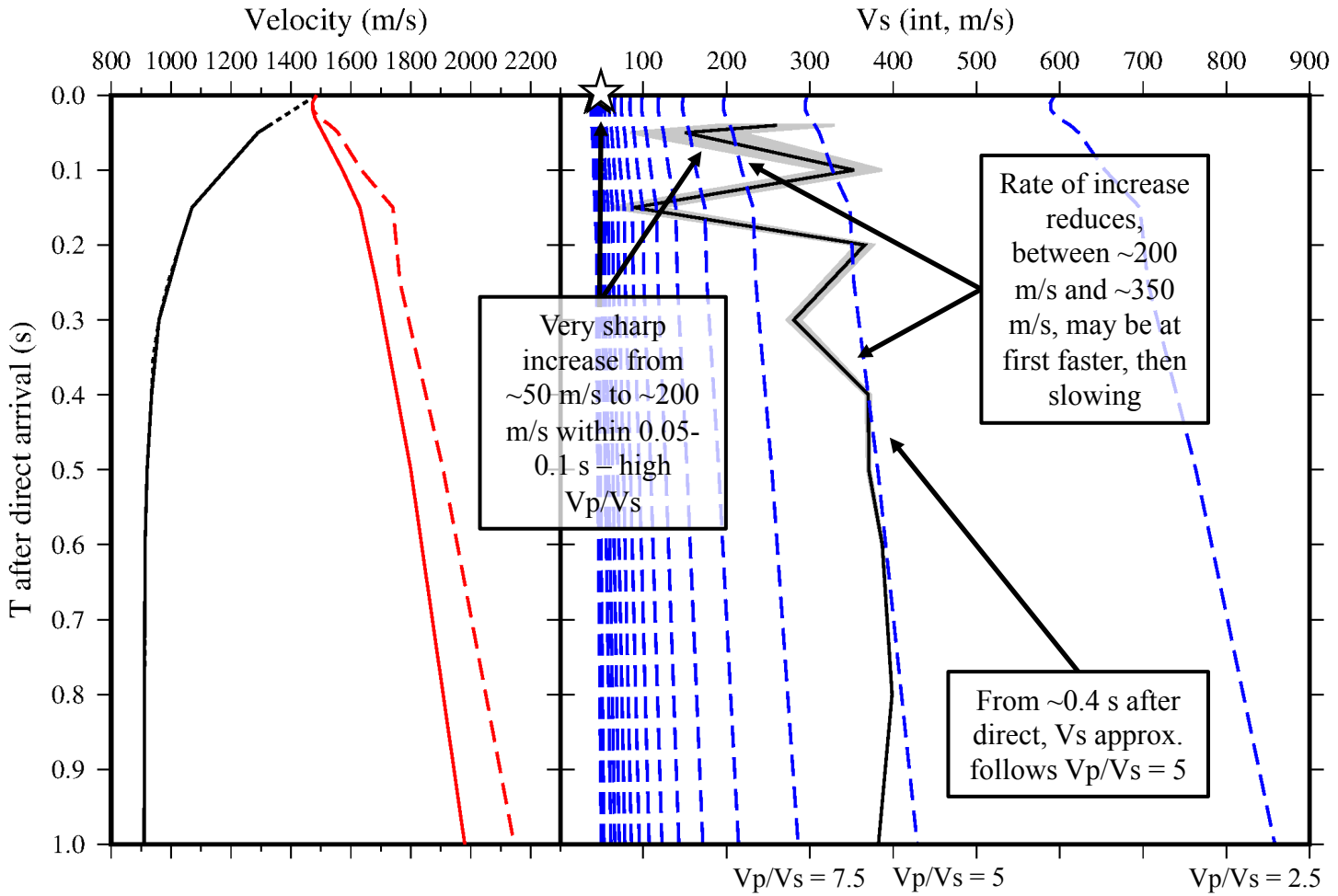

Black - Vs_{int} calculated for T_{direct} = 0.1 s, corresponding to average seabed direct arrival time around pockmark

Grey envelope shows range for T_{direct} = 0.09-0.11 s

Dashed blue lines – Vs_{int} using different Vp/Vs values, plotted at 2.5 increments

Star = North Sea soil shear velocity (Armstrong et al., 2020) – Vp/Vs ~30-37.5

Preliminary observations

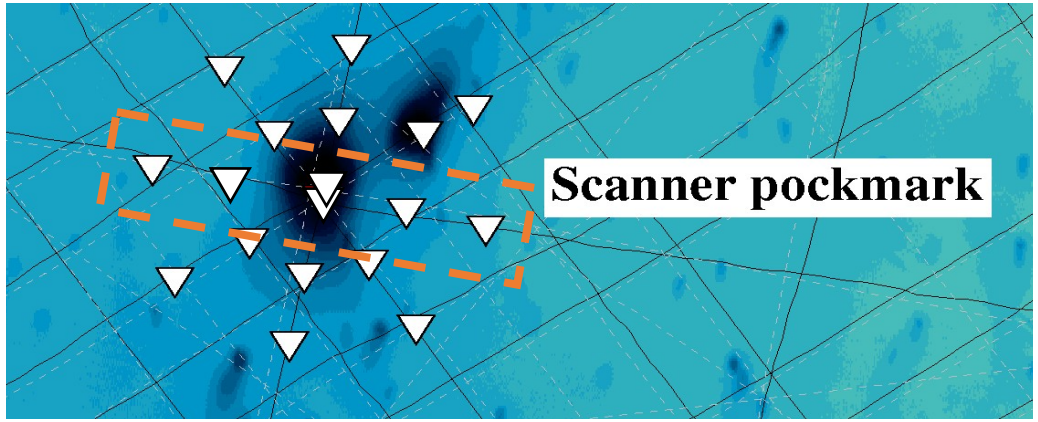

Guide to figures:

OBSs shown are, W to E, OBS 16, 5, 6, and 12.

Comprise an ~W-E section across Scanner pockmark (fig., orange box).

Data shown here are from the **GI source, transverse component** (converted to amplitude), binned at 9˚ azimuthal intervals to maximize coverage, for three frequency bands.

Vertical dashed blue lines = orientations of horizontal geophone components.

Light blue arrows = polarity reversals and amplitude nulls (dotted where less clear).

Diagrams showing approximate orientations of symmetry planes (hence, anisotropy) shown for the lower and higher frequency-band cases. Solid lines = good evidence for symmetry plane. Dashed lines = weaker evidence, or these being inferred from strong evidence at +180˚.

Only a single, depth-independent symmetry plane is identified in the first instance.

GI source, low frequencies
Transverse component
9° azimuthal bins
0-200 m shot-receiver offsets

W pockmark E

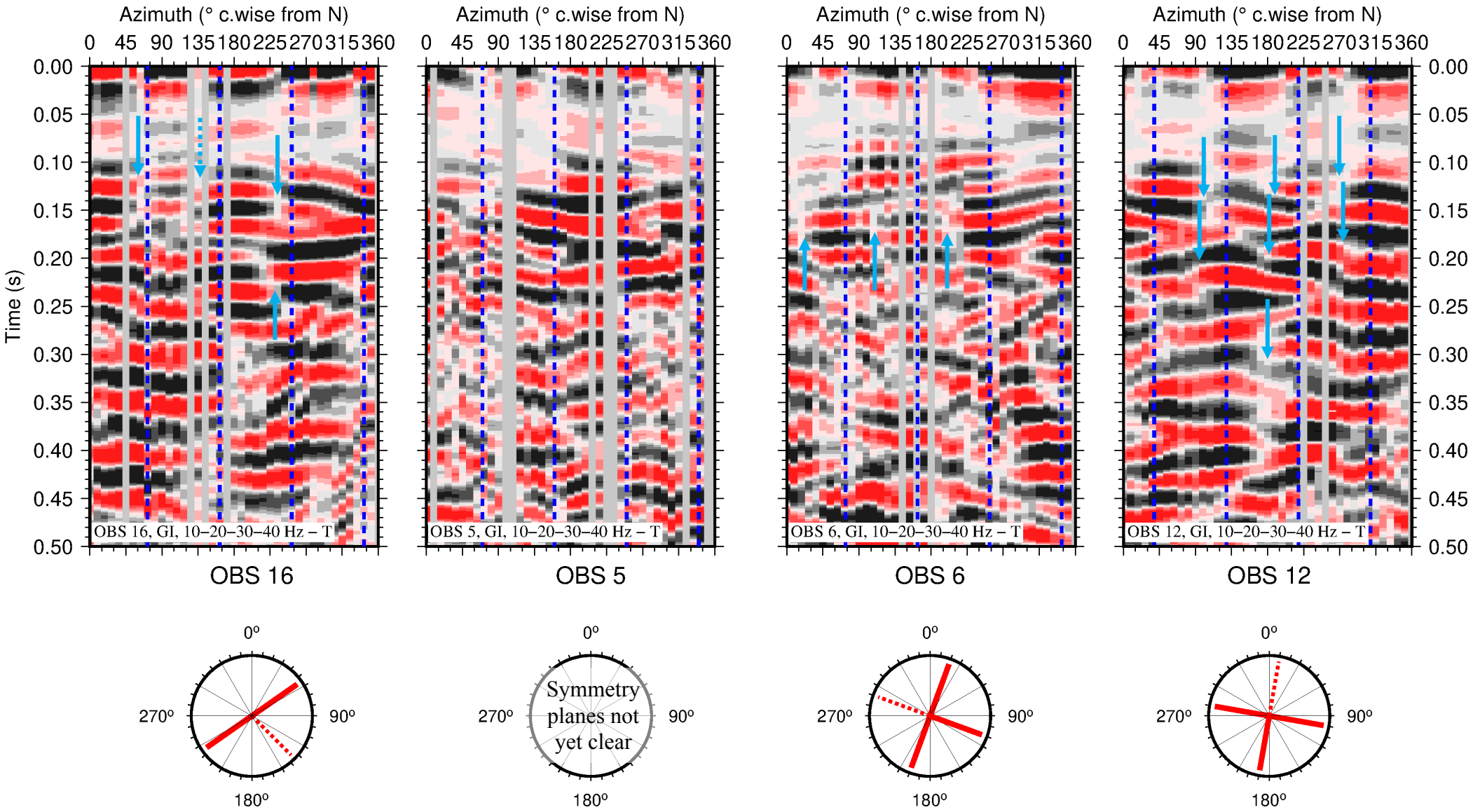

Retention of low frequency (~20-30 Hz) component does not always show full 'half-wavelength' polarity reversals or amplitude nulls.

However there is evidence for 90° separated symmetry planes, at short delays after the direct arrival at ~0.1 s for 3 of 4 OBSs.

GI source, intermediate frequencies
Transverse component
9° azimuthal bins
0-200 m shot-receiver offsets

W pockmark E

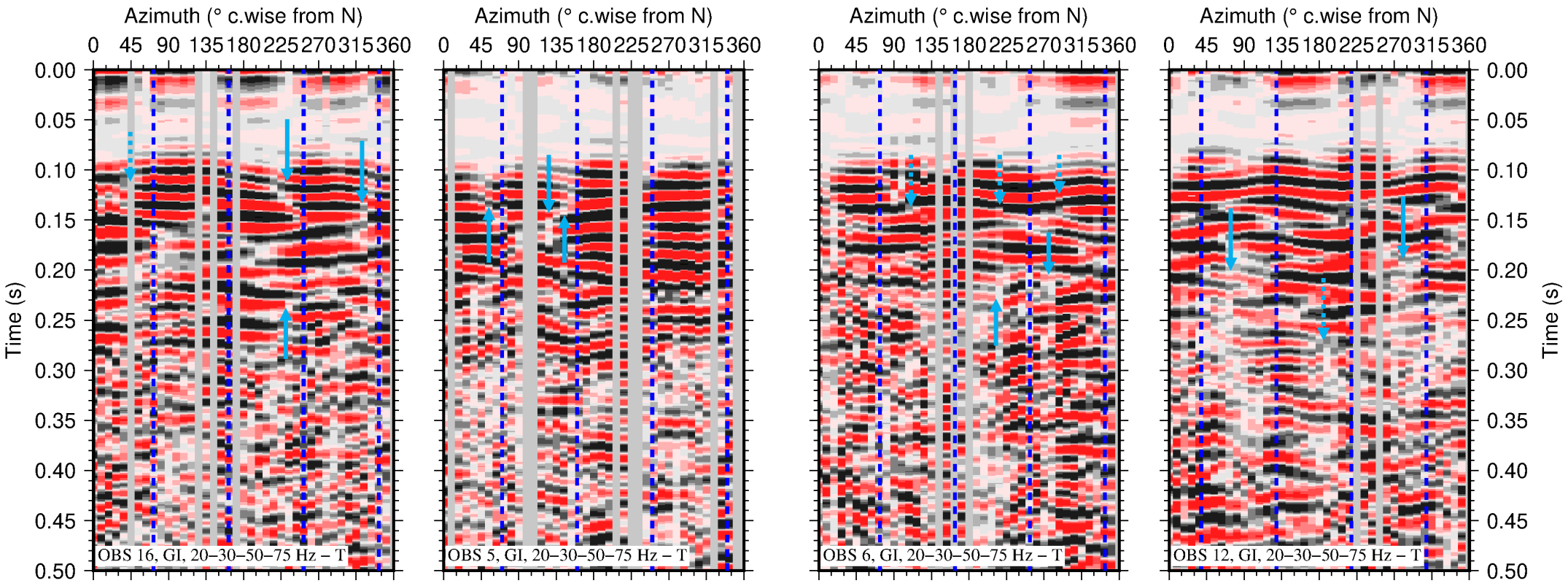

Some evidence for polarity reversals (OBS 16, 5, 6) and amplitude nulls (5, 6, 12).

Polarity reversals generally less clear than for low frequency case.

GI source, higher frequencies
Transverse component
9° azimuthal bins
0-200 m shot-receiver offsets

W pockmark E

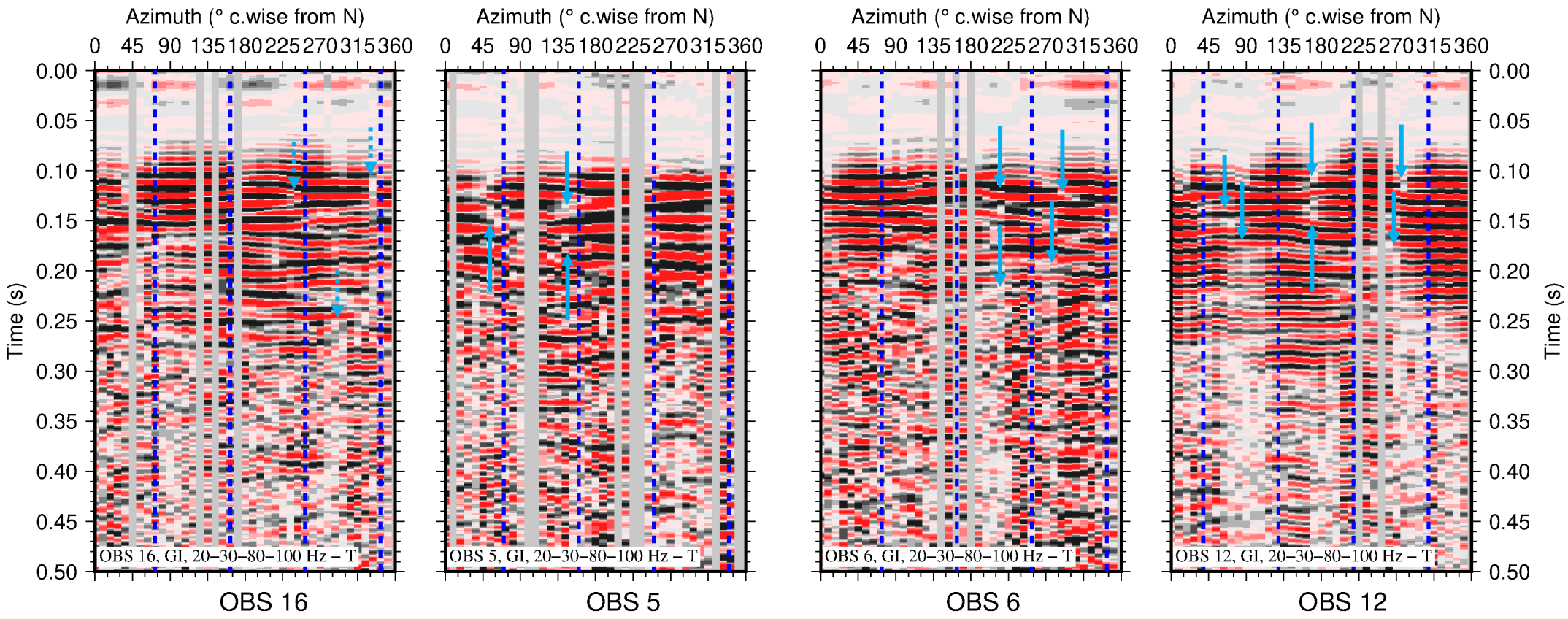

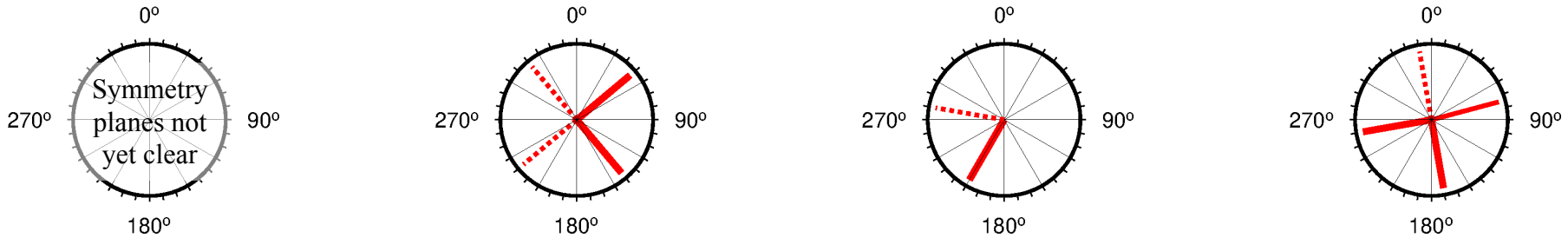

At higher frequency, polarity reversals are less clear.

Still seen at ~0.14 s in OBS5 and ~0.12 s in OBS 12.

Amplitude nulls are clear for OBSs 6 and 12.

Preliminary observations summary

- Appears to be evidence for SWS, through T component polarity reversals / amplitude nulls at 90˚ intervals.
- Occurs at short delays after direct arrival, indicating a stratigraphically shallow source.
- Evidence for SWS is not clear for all OBSs/frequencies, and further work is required to make robust anisotropy observations for different frequency bands.
- Use of limited offsets for binning and stacking introduces azimuthal coverage gaps. Further velocity analysis and offset/depth consideration may resolve this.
- Appears to be variation in the azimuths of symmetry planes across the pockmark from W to E. Further work will analyse these patterns in greater spatial detail, in addition to possible changes with depth.

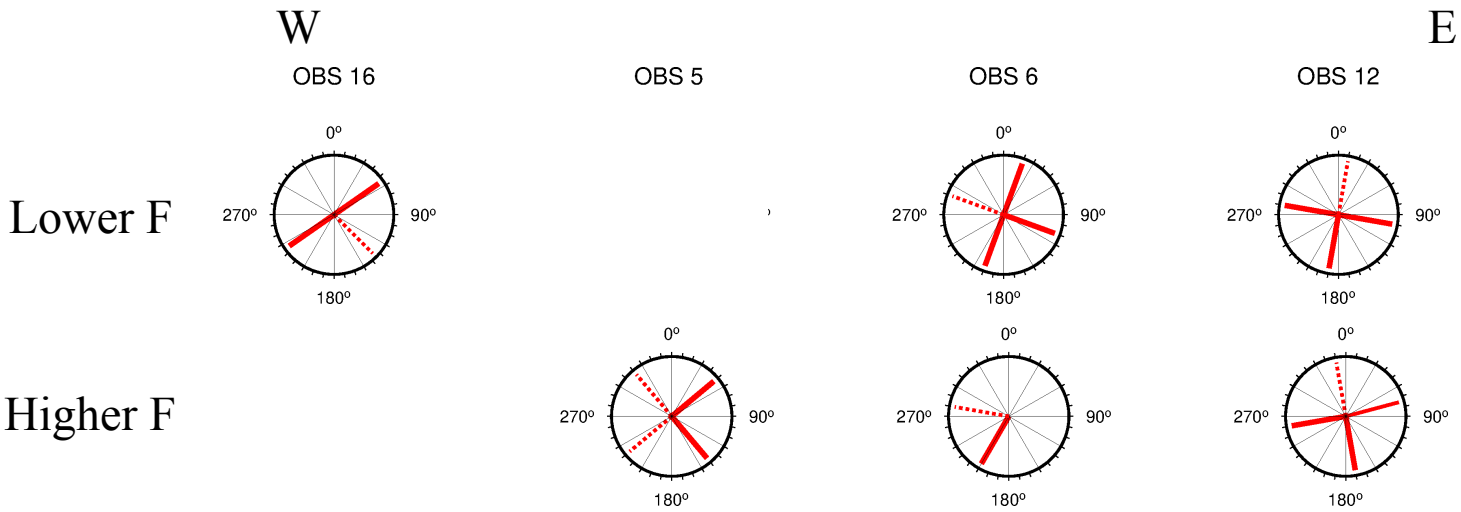

Ongoing work

- Further detailed analysis of orientations and strength of anisotropy (including uncertainties) required, including for more instrument locations (within pockmark, reference site).
- Analysis of radial components to discriminate fast and slow directions and strength of anisotropy.
- This will be assisted by further azimuthally-dependent velocity analysis, and consideration of depths of converting boundaries, to clarify offset ranges which can be used for binning and stacking data.
- If multiple orientations of anisotropy are observed at different depths, a top-down layer-stripping approach may be required (e.g. Haacke et al., 2009).
- Observations will be combined with those using higher frequency seismic sources (sparkers), to study the frequency-dependence of anisotropy.

- By comparing observations for Scanner pockmark and the reference site, we aim to further contribute to the understanding of the structures and processes governing vertical fluid migration in these environments.

References

Armstrong et al., 2020, Seismic inversion of soil damping and stiffness using multichannel analysis of surface wave measurements in the marine environment, *Geophys. J. Int.*

Bale et al. (2009), Shear wave splitting applications for fracture analysis and improved imaging: some onshore examples, *First Break*

Bull (2017) JC152 cruise report

Bull et al. (2018), Constraining Leakage Pathways Through the Overburden Above Sub-Seafloor CO_2 Storage Reservoirs. *14th Greenhouse Gas Control Technologies Conference (GHGT-14)*

Chapman, (2003), Frequency-dependent anisotropy due to meso-scale fractures in the presence of equant porosity, *Geophysical prospecting*

Dix (1955), Seismic Velocities from Surface Measurements, *Geophysics*

Exley et al. (2010), Detection of seismic anisotropy using ocean bottom seismometers: a case study from the northern headwall of the Storegga Slide, *Geophys. J. Int.*

Haacke & Westbrook (2006), A fast, robust method for detecting and characterizing azimuthal anisotropy with marine PS converted waves, and its application to the west Svalbard continental slope, *Geophys. J. Int.*

Haacke et al. (2009), Layer stripping of shear-wave splitting in marine PS waves, *Geophys. J. Int.*

Maultzsch et al., (2003), Modelling frequency-dependent seismic anisotropy in fluid-saturated rock with aligned fractures: implication of fracture size estimation from anisotropic measurements, *Geophysical Prospecting*

Stewart & Ferguson (1996) Shear-wave interval velocity from P-S stacking velocities, *CREWES Research Report, Vol. 8*

STEMM-CCS project web page - http://www.stemm-ccs.eu

CHIMNEY project web page - https://www.southampton.ac.uk/oes/research/projects/chimney.page

Contact: a.h.robinson@soton.ac.uk